Journal of Solid State Chemistry **147,** 450–463 (1999)
Article ID jssc.1999.8383, available online at http://www.idealibrary.com on IDEAL®

Incommensurate Nuclear and Magnetic Structure of the Oxygen-Deficient Perovskites $(Ba_{2-3x}Bi_{3x-1})(Fe_{2x}Bi_{1-2x})O_{2+3/2x}$ $(0.43 \leq x \leq 0.50)$

Ph. Boullay, D. Grebille, M. Hervieu, and B. Raveau

Laboratoire CRISMAT, UMR 6508-Université de Caen 6, Blvd du maréchal Juin, 14050 Caen Cedex, France

and

E. Suard

Institut Laue Langevin, Avenue des Martyrs, B.P. 156, 38042 Grenoble Cedex 9, France

Received January 8, 1999; in revised form April 30, 1999; accepted May 21, 1999

The actual nuclear and magnetic structures of the oxygen perovskites $[Ba_{2-3x}Bi_{3x-1}][Fe_{2x}Bi_{1-2x}]O_{2+3x/2}$ $(0.40 < x \leq 0.50)$ were studied combining XRPD and NPD data. The incommensurate modulated structures of the members $x = 0.45$ and $x = 0.48$ were determined in the superspace formalism. It is shown that bismuth and barium cations are not distributed at random over a single site but exhibit a particular ordering which can be described by a substitutional modulation. In such structures, the displacement of the cation from its average position is much larger for bismuth than for barium. The modulated fourfold superstructure of $Bi_2Ba_2Fe_4O_{11}$ $(x = 0.50)$, "$a_p \times a_p \times 4a_p$" is closely related to those of incommensurate phases, with a "$Bi_{1/4}Ba_{3/4}Ba_{1/4}$" ordering of the cations. Nevertheless, a certain disordering of these cations and oxygen vacancies are evidenced in the superstructure. The antiferromagnetic (AF) ordering is the same for all the members: iron spins are antiferromagnetically coupled along [110] and along [001] forming (001) AF planes. © 1999 Academic Press

INTRODUCTION

Transition metal oxides with the perovskite structure form a large family whose magnetic properties have been extensively studied (see for a review Refs. 1–3). In this respect iron-based oxides remain an important field of research for the discovery of new materials, since iron, besides its various valence states, Fe(III), Fe(IV), and Fe(V), is able to adopt various coordinations, octahedral, pyramidal, and tetrahedral. It results in a great flexibility of the perovskite framework which is susceptible to exhibit large deviations from the oxygen stoichiometry with respect to the ideal formula ABO_3.

The association of a lone pair cation, such as Bi^{3+} to iron, has allowed complex perovskites to be synthesized, in which bismuth is distributed over both A and B sites. A first series, $[Ba_{1-y}Bi_y][Fe_{1-y}Bi_y]O_{3-\delta}$, was discovered more than 20 years ago by Zanne *et al.* (4), for which the authors evidenced mixed valence states of the metallic elements. Fe(III)/Fe(IV) and eventually Bi(III)/Bi(V). Recently, we synthesized a new series of oxygen-deficient perovskites in the same Ba–Bi–Fe–O system with the fomulation $[Ba_{2-3x}Bi_{3x-1}][Fe_{2x}Bi_{1-2x}]O_{2+3x/2}$ $(0.33 < x \leq 0.5)$. The sample preparation and the overview of the structural and physical properties have been published in a previous paper (5). These compounds are characterized by the only presence of Fe^{3+} and Bi^{3+} and are weak ferromagnets with a magnetic transition between 620 and 720 K. The crystallographic study of these phases, using electron diffraction, showed their great complexity. Incommensurate satellites were indeed observed for a large composition range, $0.40 < x \leq 0.50$, corresponding to a modulation vector $\mathbf{q} = \gamma\mathbf{c}^*$, with γ ranging from 0.3 for $x = 0.40$ to 0.25 for $x = 0.50$. In fact, the particular γ value, observed for $x = 0.50$, suggests that this phase-formulated $Ba_2Bi_2Fe_4O_{11}$ may be better described as a superstructure of the perovskite, i.e., in a tetragonal supercell with $a \approx a_p$ and $c \approx 4a_p$. While quadruple perovskites oxides have already been reported with $La_2Ba_2Cu_2Sn_2O_{11}$ (6) and $La_2Ba_2Cu_2Ti_2O_{11}$ systems (7, 8), this limit compound is particular in the sense that the B sites are uniquely occupied by Fe.

The average structure of these modulated perovskites, corresponding to x ranging from 0.43 to 0.50, was previously solved in a tetragonal cell ($a \approx a_p$, $c \approx a_p$) with the space group $P4/mmm$ (5). To understand the chemistry

0022-4596/99 $30.00

and magnetism of these oxides, we have undertaken the study of their actual structure, combining X-ray powder diffraction (XRPD) and neutron powder diffraction (NPD).

SYNTHESES AND DATA COLLECTION

The compounds $(Ba_{2-3x}Bi_{3x-1})(Fe_{2x}Bi_{1-2x})O_{2+3x/2}$ were prepared by solid state reaction, at 850°C in air for 24 h, of the stoichiometric ratios of $BaCO_3$, Bi_2O_3, and Fe_2O_3, as previously reported (5). This thermal treatment was two times applied with intermediate grindings. The oxygen content was determined by redox titration. The chemical analyses of all the compounds corresponding to $0.40 \leq x \leq 0.50$ showed that there is no significant excess of oxygen with respect to the formula "$O_{2+3x/2}$"; this is in agreement with the NPD refinements, implying that bismuth and iron are both in the trivalent state.

For the structural investigation of the incommensurate structure, the members $x = 0.45$ and $x = 0.48$ with the highest intensities for the satellite reflections were chosen. To improve the statistics of the X-ray data collection, even at large 2θ values, the scan was optimized by using a nonconstant step width (smaller at low angles, larger at high angles) and a variable counting time per step (shorter at low angles, longer at high angles). The prototype 2 circles diffractometer of the CPS Laboratory at *Ecole Centrale de Paris*, equipped with a copper rotating anode, was used. To enlarge the amount of collected data, the monochromatized Cu$K\beta$ wavelength ($\lambda_1 = 1.3922$ Å for Cu$K\beta_1,\beta_3$) was used. For the member $x = 0.5$, the data collection was performed on a Seifert diffractometer using the monochromatized Cu$K\alpha_1$ wavelength ($\lambda = 1.5406$ Å) and with a nonconstant step width and a variable counting time per step method.

Neutron powder diffraction (NPD) data were collected at room temperature in the range $0° \leq 2\theta \leq 160°$ on the high-resolution powder diffractometer D1A (ILL-Grenoble) using a wavelength $\lambda = 1.909$ Å.

The Rietveld structure analysis was performed with both programs XND (9) (nuclear structure) and Fullprof (10) (magnetic structure).

The samples for electron microscopy were prepared by crushing the crystallites in alcohol. The electron diffraction study was carried out with a JEOL 200CX and JEOL 2010 electron microscopes working at 200 kV, fitted with tilting rotating sample holders. The high-resolution electron microscopy was performed with a TOPCON 002B electron microscope, operating at 200 kV, with a resolution limit of 1.8 Å ($C_s = 0.4$ mm). The three microscopes are equipped with EDS analyzers. Image calculations were carried out with the MacTempas software.

THE INCOMMENSURATE MODULATED STRUCTURES

Super Space Group and Constraints

It is now well known that incommensurate structures are better described using the superspace formalism. The super space group (SSG) was determined on the basis of the ED and XRPD observations (5). Considering the absence of conditions limiting the reflection in the subcell system, the SG $P4/mmm$ corresponding to the highest symmetry has been chosen and the associated Bravais class in R^4 is (4/*mmm*, 1-111) (11). The satellites can be indexed considering a modulation vector $\mathbf{q} = \gamma\mathbf{c}^*$ and the SSG would therefore be in the form $P4/mmm(00\gamma)$. Since no condition is observed for the satellites, the SSG $P4/mmm(00\gamma)1\text{-}111$ is retained.

For each of the atoms, the displacement with regard to the mean position in the nth cell is expressed through the $\mathbf{u}_n$ vector with

$$\mathbf{u}_n = \sum_l \mathbf{A}_l \cos[2\pi l\mathbf{q}\cdot\mathbf{r}_n^0] + \sum_l \mathbf{B}_l \sin[2\pi l\mathbf{q}\cdot\mathbf{r}_n^0],$$

where $\mathbf{r}_n^0$ is the mean position of the atom in the nth cell and l the order of the harmonic. The vector $\mathbf{A}_l$ is expressed by

$$\mathbf{A}_l = \sum_{i=1}^{3} A_{li}\mathbf{a}_i$$

with $\mathbf{a}_1 = \mathbf{a}$, $\mathbf{a}_2 = \mathbf{b}$, and $\mathbf{a}_3 = \mathbf{c}$ (similarly for $\mathbf{B}_l$). The site occupancy is represented by

$$\mathbf{P}_n = \sum_l \mathbf{C}_l \cos[2\pi l\mathbf{q}\cdot\mathbf{r}_n^0] + \sum_l \mathbf{D}_l \sin[2\pi l\mathbf{q}\cdot\mathbf{r}_n^0].$$

The modulation functions will be represented using the internal parameter $t = x_4 - \mathbf{q}\cdot\mathbf{r}$, which allows one to give a continuous description of the modulation functions and where x_4 represents the internal coordinate defined by $x_4 = \mathbf{q}\cdot\mathbf{r}_n^0$.

All the atoms are located in special positions 4/*mmm* so that the symmetry constraints impose that only the B_{13} value, corresponding to a displacement along the c axis, and the C_1 value, corresponding to a modulation of occupancy along the c axis, could be refined.

X-Ray Powder Diffraction

The value of the irrational component of the modulation vector was refined respectively for the members $x = 0.45$ and $x = 0.48$ to $\gamma = 0.2883(7)$ and $\gamma = 0.2721(8)$ in agreement with the ED observations. The chemical composition was fixed considering EDS analyses and chemical analyses

TABLE 1
$x = 0.45$ Member: Results of the Rietveld Analysis (X Rays) of the Incommensurate Modulated Structure

Space group: $P4/mmm(00\gamma)1\,\bar{1}\,1\,1$, $a = 4.014(1)$ Å, $c = 4.085(1)$ Å, and $\mathbf{q} = \gamma\mathbf{c}^* = 0.2883(7)\mathbf{c}^*$

Atom	x	y	z	Site	B_{iso} (Å^2)	Occup.
Ba	0	0	0	1*a*	3.4(2)	0.63[a]
Fe	0.5	0.5	0.5	1*d*	0.2(2)	0.94[a]
O(1)	0.5	0.5	0	1*c*	1.7(6)	0.89(4)
O(2)	0.5	0	0.5	2*e*	1.7(6)	0.90(4)

Modulation parameters

Atom	B_{13}	B_{23}	C_1	C_2
Ba	0.0593(1)	0.0253(3)	− 0.095(2)	− 0.023(4)
Fe	0.0140(2)	—	− 0.0608(8)	—

R values

R_{wp}	GofF	R_{Bragg}	R_F	R_{F0}	R_{F1}	R_{F2}
8.9%	1.8	8.3%	12.1%	5.4%	20.4%	27.1%

[a]Fixed values (completed to 1 by bismuth).

(5). Only the relative distribution of the oxygen onto the two anionic sites was refined. The isotropic thermal factors for the oxygen are refined and are considered as equal for both O(1) and O(2) sites. The results of the refinements are presented in Tables 1 and 2; the XRPD diagrams for the compounds $x = 0.45$ and $x = 0.48$ were previously reported in (5).

TABLE 2
$x = 0.48$ Member: Results of the Rietveld Analysis (X Rays) of the Incommensurate Modulated Structure

Space group: $P4/mmm(00\gamma)1\,\bar{1}\,1\,1$, $a = 3.9950(4)$ Å, $c = 4.0903(7)$ Å, and $\mathbf{q} = \gamma\mathbf{c}^* = 0.2721(8)\mathbf{c}^*$

Atom	x	y	z	Site	B_{iso} (Å^2)	Occup.
Ba	0	0	0	1*a*	2.09(6)	0.57[a]
Fe	0.5	0.5	0.5	1*d*	0.5(1)	0.96[a]
O(1)	0.5	0.5	0	1*c*	2.2(4)	0.93(3)
O(2)	0.5	0	0.5	2*e*	2.2(4)	0.88(3)

Modulation parameters

Atom	B_{13}	B_{23}	C_1	C_2
Ba	0.0639(1)	0.0328(2)	− 0.218(2)	− 0.042(3)
Fe	0.0081(2)	—	− 0.04[a]	—

R values

R_{wp}	GofF	R_{Bragg}	R_F	R_{F0}	R_{F1}	R_{F2}
6.4%	1.6	7.2%	7.9%	4.5%	11.1%	14.8%

[a]Fixed values. (completed to 1 by bismuth).

TABLE 3
Average Structure of $x = 0.45$ and $x = 0.48$ Members (Rietveld Analysis, Combined X Rays/Neutrons)

Space group. $P4/mmm$ (No. 123)

Site	x	y	z	Pos. Wyckoff
A	0.5	0.5	0.5	1*d*
B	0	0	0	1*a*
O(1)	0.5	0.5	0	1*c*
O(2)	0.5	0	0.5	2*e*

$x = 0.45$: $a = 4.0146(2)$ Å and $c = 4.0845(5)$ Å

Site	B_{eq} (Å^2)	u_{11}	u_{33}		Occup.
B	4.2	0.036(3)	0.089(7)	Ba/Bi:	0.63(2)/0.37(2)
A	1.3	0.016(2)	0.016(4)	Fe/Bi:	0.94(2)/0.06(2)
O(1)	2.1	0.033(5)	0.016(7)		0.9
O(2)	1.7	0.020(3)	0.027(5)		0.9

XR: Gof = 2.3, $R_{wp} = 11.1\%$, $R_{Bragg} = 12.2\%$, $R_F = 26.2\%$
Neutron: Gof = 2.1, $R_{wp} = 8.7\%$, $R_{Bragg} = 6.6\%$, $R_F = 4.3\%$

$x = 0.48$: $a = 3.9954(7)$ Å and $c = 4.090(1)$ Å

Site	B_{eq} (Å^2)	u_{11}	u_{33}		Occup.
A	4.7	0.028(3)	0.12(1)	Ba/Bi:	0.57(2)/0.43(2)
B	1.2	0.014(3)	0.019(6)	Fe/Bi:	0.96(2)/0.04(2)
O(1)	2.5	0.035(8)	0.03(1)		0.9
O(2)	1.9	0.017(4)	0.039(9)		0.9

XR: Gof = 2.2, $R_{wp} = 8.6\%$, $R_{Bragg} = 10.0\%$, $R_F = 14.1\%$
Neutron: Gof = 2.2, $R_{wp} = 10.2\%$, $R_{Bragg} = 9.2\%$, $R_F = 7\%$

The reliability R_{F0} factors for the main reflections as well as the global R_F factors is greatly improved compared to the R_F factors obtained in the average structure study (see Table 3). Concerning the description of the modulated structure, only the reliability factors obtained for the compound $x = 0.48$ are good enough to be considered as significant. Still, it is noticeable that the structural results reached for the two refinements are in agreement and confirm some structural characteristics already suggested by the average structure study (5).

The evolution of the positions, occupancies, and distances versus the internal parameter shows that the *A* site is strongly affected by the periodic deviation (maximum displacement of 0.3 Å for $x = 0.45$ and of 0.35 Å for $x = 0.48$), in contrast to the *B* site (displacements of 0.06 Å and 0.03Å, respectively). But looking more carefully, some results tend to prove that our model needs to be improved, in particular, for the description of the structure in $t = 0$ or $t = 0.5$, and for the correlation between occupancy and displacements modulations.

To get a better description, we have focused our study on the member $x = 0.48$ and tried to combine the information

TABLE 4
$x = 0.48$ Member: Results of the Rietveld Analysis (Combined X-Rays PD and Neutrons PD) of the Incommensurate Modulated Structure

Space group: $P4/mmm\,1\,\bar{1}\,1\,1(00\gamma)$, $a = 3.9957(4)$ Å, $c = 4.0906(7)$ Å, and $\mathbf{q} = \gamma\mathbf{c}^* = 0.2719(8)\mathbf{c}^*$

Atom	x	y	z	Site	B_{iso}(Å^2)	Occup.
Ba	0	0	0	1*a*	2.04(5)	0.57[a,b]
Fe	0.5	0.5	0.5	1*d*	1.1(1)	0.96[a,b]
O(1)	0.5	0.5	0	1*c*	1.8(4)	0.82(3)
O(2)	0.5	0	0.5	2*e*	1.9(2)	0.93(3)

Modulation parameters

Atom	B_{13}	B_{23}	C_1	C_2	C_3
Ba	0.0701(1)	0.0460(2)	− 0.248(2)	—	− 0.182(2)
Fe	0.0131(2)	0.0114(3)	− 0.04[a]	—	—
O(1)	− 0.0102(7)	− 0.0027(9)	—	—	—
O(2)	− 0.0470(3)	− 0.0107(5)	—	—	—

R values

	R_{wp}	GofF	R_{Bragg}	R_F	R_{F0}	R_{F1}	R_{F2}	R_{F3}
RX	6.8%	1.7	8.4%	8.4%	5.3%	9.8%	13.5%	13.1%
N	9.1%	2.0	11.9%	10.1%	5.2%	18.0%	61.8%	24.8%

[a]Fixed values.
[b]Completed to 1 by bismuth.

from NPD together with the XRPD data to account for oxygen displacements and occupancy.

Combined XRPD and NPD

At this second stage of the study, all the atoms are considered as displacively modulated. The isotropic thermal factors for the oxygen atoms are now refined independently. During the first step of the refinement, the values taken by the C_1 and C_3 parameters for the A site appear to give an occupancy slightly greater than 1. The sum $C_1 + C_3$ was then fixed and only the ratio C_1/C_3 was refined. The final results obtained for this refinement are given in Table 4; the XRPD and NPD diagrams are represented in Figs. 1 and 2, respectively. The evolution of the positions, occupancy, and distances versus the internal parameter t are represented in Fig. 3.

Compared to XRPD data, the reliability factors are satisfactory and the results are close to the expectation. Nevertheless, for the NPD data, the reliability factors concerning the satellite reflections are poor, suggesting that the description of the oxygen modulation is not properly done. Most importantly, we can mention two parameters that prevent us to get better reliability R factors. Firstly, there exist some extra magnetic peaks which cannot be taken into consideration by the program XND.[1] and, secondly, the statistic of the NPD data are not as good as for the XRPD data. Both factors would affect the reliability by reducing the number of significant true satellites reflections.

For the oxygen atoms, once again we observed a confirmation of the hypothesis made after the average structure study (5). Indeed, the O(2) position is much more affected by the periodic deviation than the O(1) position with a maximum displacement of 0.2 Å compared to 0.02 Å for O(1). Following the results of the average study, some displacements may exist for the O(1) position but the study of the modulated structure shows that these displacements are apparently not related to a periodic deviation along the **c** direction. At this point of the study the O(1) position is then considered as affected mainly by some static disorder.

For the cations, the structural model is compatible with the previous one but with a general increase in the amplitude of the modulation. A second-order term was added to describe the displacive modulation for the B site. The maximum displacement for this site is now 0.1 Å and, considering the oxygen displacements, the six B–O distances are ranging from 1.9 to 2.15 Å. In the zone around $t = 0.35$, where the B site is fully occupied by Fe, the Fe–O distances range from 2.0 to 2.1 Å which is suitable for Fe.

For the occupancy modulation of the A site, we now obtain a fully occupancy by Ba for $t = 0.5$, using the third order (C_3) in the harmonic function instead of the second order. The t range, from 0.35 to 0.65, corresponds to a zone where Ba mostly occupies the A site in association with very small modulated displacements. For this region, the A cation is surrounded by 12 oxygen atoms with A–O distances ranging from 2.8 to 2.95 Å, which indeed corresponds to a suitable Ba environment (Fig. 4a). When the A site begins to be preferentially occupied by Bi, the A-position displacement correlated with the one observed for O(2) allows one to get a stronger decrease of the A–O distances than the one obtained in the alone XRPD study. The lowest A–O distances are about 2.45 Å for the values $t = 0.15$ and $t = 0.85$, which corresponds to a maximal displacement of 0.4 Å from the average position and a coordination number of 4 (Fig. 4b). Around $t = 0$, the A site is almost totally occupied by Bi, but still this corresponds to a region where the modulated displacement is low, resulting for the t values $[0, 0.1]$ and $[0.9, 1]$ in an abnormal increase of the Bi–O distances and coordination number. To explain such a singularity, we propose that the displacive modulation cannot be properly described using a harmonic function but looks rather like a straight line, i.e., a discontinuous function as represented in Fig. 5. Unfortunately, the use of such functions is not possible in the program XND. By extrapolation of the actual model, it is reasonable to expect some Bi–O

[1] Only the strongest magnetic reflections were entered as parasitic reflection.

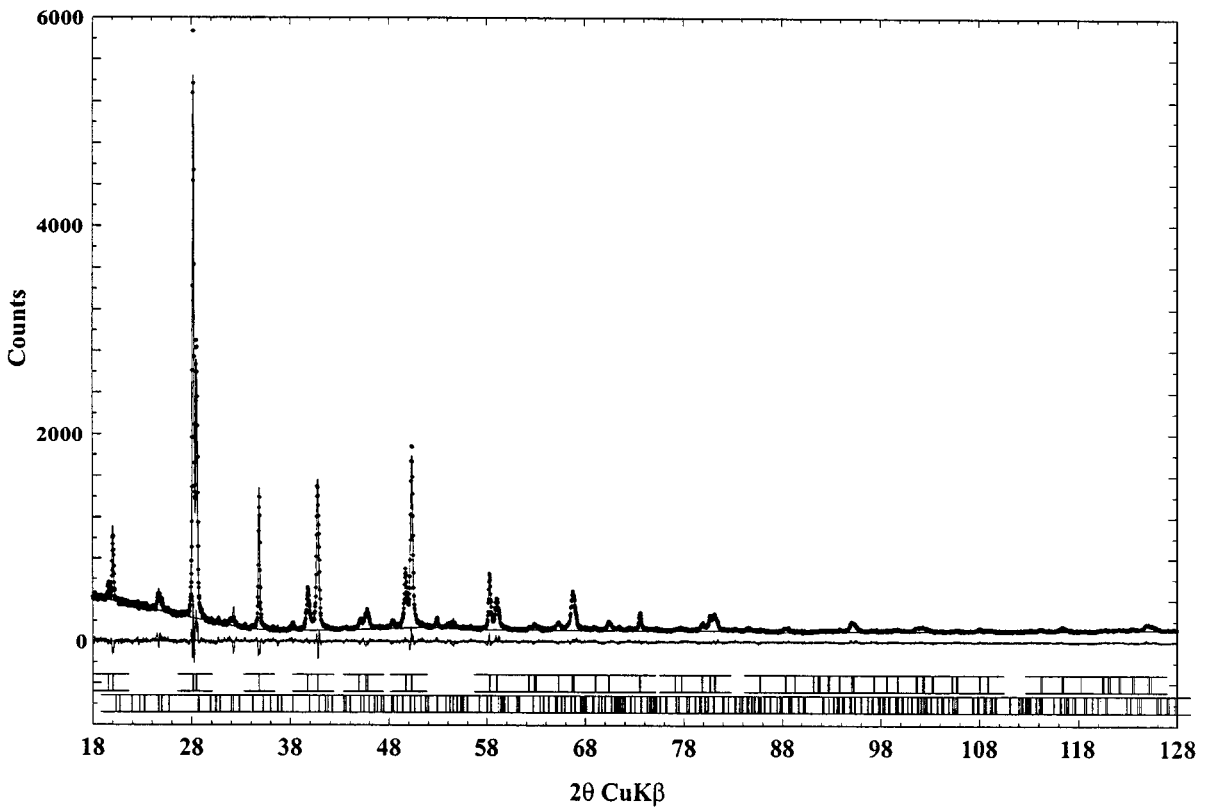

FIG. 1. XRPD diagram of the compound $x = 0.48$. The first row of bars indicates the basic reflections and the second row the satellites reflections.

distances around 2.3 Å for a 100% Bi occupancy at $t = 0$. These distances are very close to the ones expected for Bi–O distances. The coordination number of 4 can locally be reduced to 3, considering both the existence of anionic vacancies as well as Bi displacements in the (a, b) plane. The environment of the Bi atoms (Fig. 4b) can then be close to the BiO_3–Lp tetrahedron, as usually observed for the Bi^{3+} ion (12).

THE QUADRUPLE PEROVSKITE: $Bi_2Ba_2Fe_4O_{11}$

A Four-Fold Superstructure

Using XRPD data, we have tested various possibilities including structures with and without mixed Ba/Bi sites. The detailed results will not be published, but these tests reveal first that models with mixed Ba/Bi sites are statistically better than the ones involving a single occupancy. Second, among the "mixed models" several possibilities appear to be statistically equivalent. Considering the compound as a four-fold superstructure, we end up with a situation where several structural models seem equally probable. To overcome this situation, we will start from the result previously obtained for the incommensurate members when $x < 0.5$.

A Commensurate Modulated Structure

All the observations made for this perovskite family indicate that the members slightly evolve from an incommensurate phase to a commensurate one for $x = 0.5$ (5). The structure of the limit commensurate member should then be closely related to the model proposed for the incommensurate structure. In this approach, we will consider the member $Bi_2Ba_2Fe_4O_{11}$ ($x = 0.5$), as a commensurate structure in $a_p \times a_p \times a'_p$ with $\mathbf{q} = 0.25\mathbf{c}^*$. Unfortunately, the program XND cannot treat in a rigorous way the commensurate modulated cases. In practice, we will work on models in "$a_p \times a_p \times 4a_p$" but only those compatible with the modulated structure described above. Thus, the displacement and occupancy modulation for the A site are described using sawtooth-type functions (Fig. 5). At $t = 0$, there exists a Bi site and, at $t = \frac{1}{2}$, a Ba site; the displacement from the average position is zero when the A site is fully occupied by Ba and maximal for Bi.

The first step consists of determining which sections of the SSG $P4/mmm(00\gamma)1$-111 are compatible with a commensurate structure with the SG $P4/mmm$ (evidenced by both XRPD and ED techniques (5)). Using the method described by Dam and Janner (13), it appears that only the sections corresponding to $t = n/8$ (n integer) satisfy this condition.

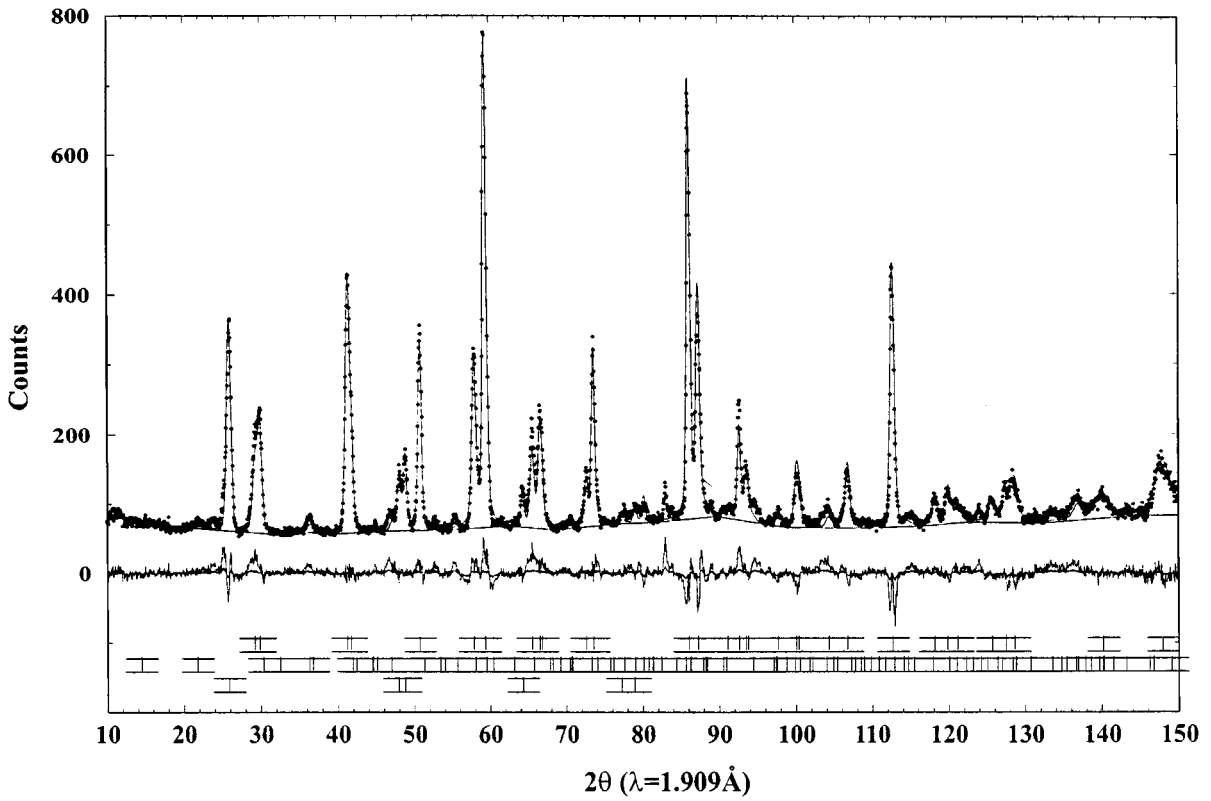

FIG. 2. NPD diagram of $x = 0.48$. The first row of bars indicates the basic reflections, the second the satellites reflections, and the third the main magnetic reflections.

Then only two possibilities have to be considered for a model in $a_p \times a_p \times 4a_p$: the one corresponding to the sections $t = 0$, $\frac{1}{4}$, $\frac{1}{2}$, and $\frac{3}{4}$ (model I) and the one for $t = \frac{1}{8}$, $\frac{3}{8}$, $\frac{5}{8}$, and $\frac{7}{8}$ (model II). For model I, the "chemical composition" of the A sites along the **c** direction varies with the sequence–Bi–($Bi_{0.5}Ba_{0.5}$)–Ba–($Bi_{0.5}Ba_{0.5}$) involving three distinct A sites. In the SG $P4/mmm$, this model can be obtained by placing the origin of the cell on a A-type cation (see Fig. 6a). For model II, the "chemical composition" of the A site varies according to the sequence–$Bi_{0.25}Ba_{0.75}$–$Bi_{0.75}Ba_{0.25}$–involving two distinct A sites. This situation can be realized by placing Fe at the origin of the cell (Fig. 6b). The two models were tested using simultaneously the XRPD and NPD data, combined in the Rietveld refinement. The oxygen positions were considered as fully occupied and all the thermal parameters will be refined using anisotropic factors. The Rietveld refinement of these two possibilities indicates that the model II, with better reliability factors (R_{Bragg}–$N = 6.6\%$ vs 7.1% and R_{Bragg}–$RX = 7.1\%$ vs 8.8%), has to be retained.

A Disordered Superstructure

The main crystallographic parameters obtained for the model II are displayed in Table 5. From the anisotropic thermal factor, we can obtain information about the location of the oxygen vacancies and the preferential direction for the atomic displacement, (a, b) plane or **c** axis. This information is summarized for each atomic position in Table 5.

With the help of the ORTEP drawing displayed in Fig. 7, the existence of two "regions" in the crystal is clearly evidenced. For the zone where the A site is mainly occupied by Ba, A(1) site, the iron and oxygen atoms have low thermal factors either isotropic, Fe(1), Fe(2), and O(4), or anisotropic, O(1). In contrast, when the A site is mainly occupied by the Bi (A(2)) site, the iron Fe(3) and oxygen atoms, O(3), O(5), and O(2), have high thermal factors revealing the existence of a region inside the crystal with important static disorders. The oxygen vacancies sit in this "disordered" region of the crystal. The O(3) and O(5) sites, with huge thermal factors ($B_{eq} \sim 9\text{Å}^2$), are indeed certainly deficient. The Rietveld analyses indicate that the best R values are obtained when the vacancies are equally placed on both O(3) and O(5) sites. In both regions, the mixed A sites are affected by a strong static disorder with a preferential displacement along the **c** direction. In this case, one has to consider that the two A sites located in (0.5, 0.5, z:2h) are actually composed of a sum of (2h) sites separated by Δz.

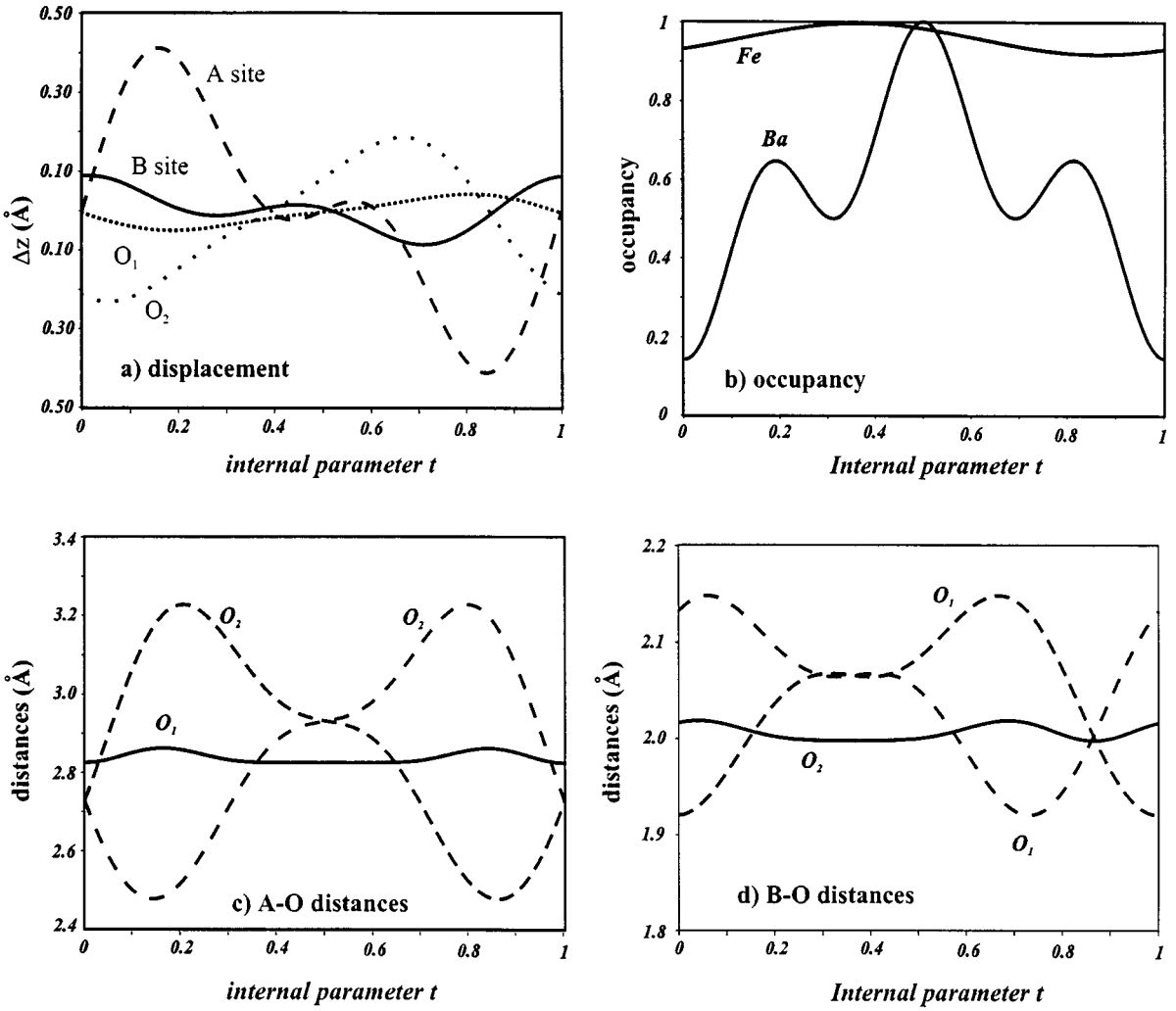

FIG. 3. Evolution of the positions, occupancy, and distances versus the internal parameter for $x = 0.48$.

The actual description, using a statistical occupancy for the A sites, does not rend an account of the microscopic situation where the local environments of Ba and Bi atoms have to be different. In an attempt to obtain a more "realistic" description, we will try to decompose the two components of the "pseudo atoms" Ba/Bi. The final refinement takes into consideration all the above remarks: the Ba and Bi components of both pseudo atoms are constrained to the same displacement and same thermal parameters. The O(3) and O(5) sites with very high thermal factors are oxygen deficient and displaced from the mirror m_x and m_{x-y}, respectively. The results of the refinement are presented in Table 6, the XRPD and NPD diagrams in Figs. 8 and 9, respectively. Interatomic distances are displayed in Table 7.

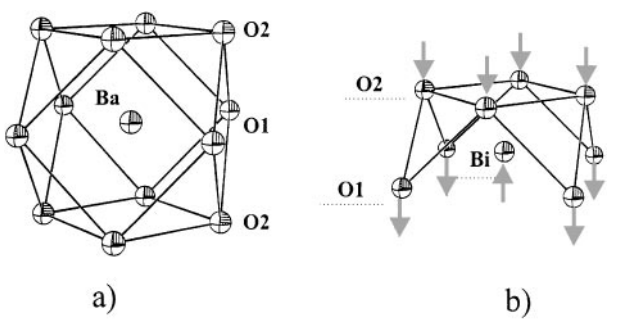

FIG. 4. (a) Ba environment: 12A–O distances ranging from 2.8 to 2.95 Å. (b) Bi environment: the lowest A–O distances ≈ 2.45 Å for $t = 0.15$ and $t = 0.85$ corresponds to a maximal displacement of 0.4 Å from the average position and, consequently, to a coordination number of 4.

The coordination number and the A–O distances are significantly lower for Bi than for Ba, but only the Ba(1) site, with 12 oxygen neighbors ranging between 2.82 and 3.05 Å, and the Bi(2) site, with 4 oxygen neighbors at 2.48 Å, are close to what we expected for these atoms. With the important static disorder observed for Bi, the exact local environment of Bi atoms cannot be obtained from this study, but the Bi atoms are undoubtedly strongly displaced from the

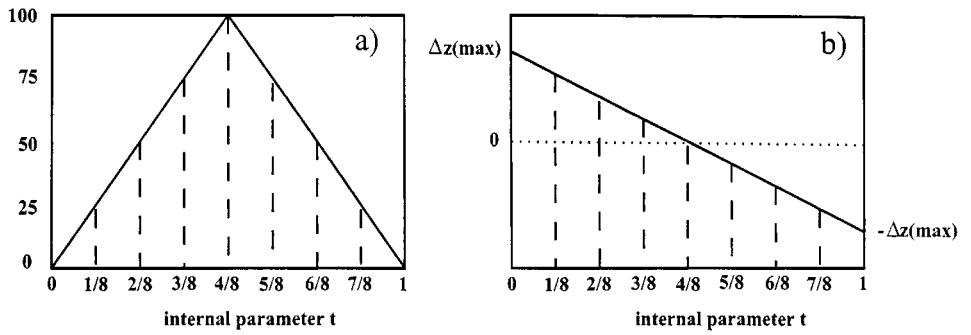

FIG. 5. Displacement and occupancy modulation for the *A* site using saw tooth-type functions.

average position given here. The Ba(2) and Bi(1) sites, which in the model are representative of the possibility to have faults in the sequence |Ba|Bi|Bi|Ba| along the **c** direction, cannot be considered as proper sites neither for Bi nor for Ba. The appearance of stacking faults in the sequence |Ba|Bi|Bi|Ba| does not seem to be the major reason for the observation of mixed Ba/Bi sites. If we suppose that the |Ba|Bi|Bi|Ba| sequence is respected along the **c** direction, the appearance of mixed macroscopic Ba/Bi sites can result from displacements along the **c** direction of adjacent |Ba|Bi|Bi|Ba| rows.

Concerning the Fe atoms, valence calculations based on the obtained bond lengths indicate that the three sites are in agreement with the only presence of Fe(III). For the Fe(1) position, located in the nondisordered region of the crystal, the coordination is 6 octahedral and quasi symmetric. Considering the oxygen deficiency for the O(5) site, the coordination of Fe(2) is either $5+1$ octahedral with a long Fe(2)–O(5) distance or 5 pyramidal (25%). The exact coordination of the Fe(3) is difficult to estimate since this position is fully located in the disordered region of the crystal. Surrounded by two deficient oxygen sites, O(3) and O(4), the Fe(3) position corresponds to a lower coordination for the iron, either 5 or 4.

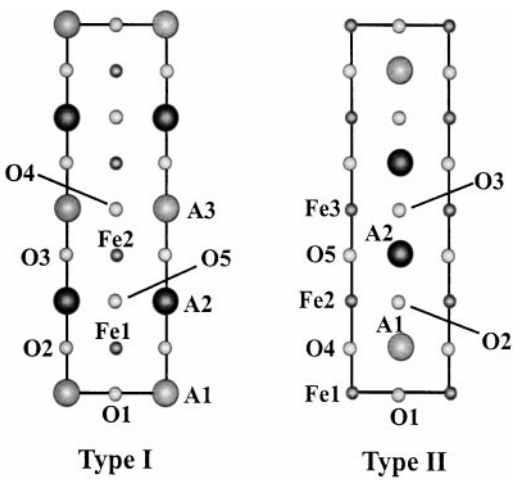

FIG. 6. (a) Model I obtained by placing the origin of the cell on a *A*-type cation. (b) Model II, obtained by placing Fe at the origin of the cell.

TABLE 5
$Bi_2Ba_2Fe_4O_{11}$ ($x = 0.5$): Structural Parameters for the Model II Type

SG: *P*4/*mmm* (No. 123), $a = 3.9804(2)$ Å, and $c = 16.378(1)$ Å
R_{Bragg}(Neutrons) = 6.6% R_{Bragg}(X rays) = 7.0%

Site	*A*(1)	*A*(2)	Fe(1)	Fe(2)	Fe(3)
	$Ba_{0.75}Bi_{0.25}$	$Bi_{0.75}Ba_{0.25}$			
Wyckoff positions	2*h*	2*h*	1*a*	2*g*	1*b*
z	0.116(1)	0.357(1)	0	0.243(1)	0.5
u_{11}	0.026(4)	0.046(4)	0.008(4)	0.015(3)	0.047(7)
u_{33}	0.081(9)	0.10(1)	0.008(7)	0.018(7)	0.04(1)
u_{11}/u_{33}	0.32	0.45	0.94	0.83	1.01
B_{eq}	3.5	5.1	0.6	1.3	3.4
Thermal factors					
Isotropic	—	—	*x*	*x*	*x*
Anisotropic	*x*	*x*	—	—	—
Static disorder	*c*	$c + (a, b)$	—	—	*x*

Site	O(1)	O(2)	O(3)	O(4)	O(5)
Wyckoff positions	2*f*	4*i*	2*e*	2*g*	2*g*
z	0	0.262(1)	0.5	0.127(1)	0.384(2)
u_{11}	0.020(4)	0.011(3)	0.11(1)	0.016(3)	0.14(1)
u_{33}	0.005(8)	0.048(9)	0.12(3)	0.017(5)	0.05(2)
u_{11}/u_{33}	3.77	0.23	0.9	0.95	2.8
B_{eq}	1.2	1.8	8.9	1.3	8.7
Thermal factors					
Isotropic	—	—	*x*	*x*	–
Anisotropic	*x*	*x*	—	—	*x*
Static disorder	—	*c*	Vacancy	—	(a, b)

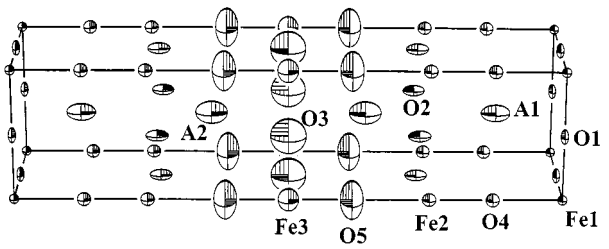

FIG. 7. ORTEP drawing of the $Bi_2Ba_2Fe_4O_{11}$ ($x = 0.5$).

Electron Microscopy

The high-resolution electron microscopy study was carried out for the $\mathbf{x} = 0.5$ sample with the quadruple perovskite structure and the $x = 0.45$ which exhibits an incommensurate modulation with $\mathbf{q} = 0.29\mathbf{c}^*$. The [100] through focus series, recorded for numerous crystallites of each of the two samples, confirmed their homogeneity.

For the $x = 0.5$ sample, the superstructure $4a_p$ generates a modification of the contrast (Fig. 10), with regard to the classical images of the perovskite-like structures, which is clearly visible for most of the focus values. However, a direct correlation of these contrast variations with structural phenomena is tricky since atomic displacements and electron density variations are concomitantly implied, which are all responsible for possible drastic contrast variations. To get additional information which would allow one to interpret our experimental images, theoretical images were calculated on the basis of the different models considered in the course of the XRPD and NPD refinements. The simulated through focus series were indeed carried out for different crystal thicknesses and for different cation distributions but also for different thermal factors. In fact, most of the calculated images are common to the different models. However, it was

TABLE 6
$Bi_2Ba_2Fe_4O_{11}$ ($x = 0.5$): Structural Parameters Obtained by Considering Two Distinct Sites "Ba" and "Bi"

SG: *P4/mmm* (No. 123), $a = 3.9804(2)$ Å, and $c = 16.378(1)$ Å

Atom	x	y	z	Site	Occup.	B(Å^2)
Ba(1)	0.5	0.5	0.122(1)	2*h*	0.75	2.6[a]
Bi(1)	0.5	0.5	0.1036(8)	2*h*	0.25	5.2[a]
Bi(2)	0.5	0.5	0.3536(8)	2*h*	0.75	5.2[a]
Ba(2)	0.5	0.5	0.372(1)	2*h*	0.25	2.6[a]
Fe(1)	0	0	0	1*a*	1	0.7[a]
Fe(2)	0	0	0.2429(4)	2*g*	1	1.2[a]
Fe(3)	0	0	0.5	1*b*	1	3.5[a]
O(1)	0.5	0	0	2*f*	1	1.4[a]
O(2)	0.5	0	0.2629(5)	4*i*	1	1.9[a]
O(3)	0.5	−0.080(4)	0.5	4*o*	3/8	2.0(4)
O(4)	0	0	0.1263(9)	2*g*	1	1.9[a]
O(5)	0.074(8)	0	0.384(1)	8*s*	3/16	1.5(8)

	Xrays	Neutrons
Gof	1.23	2.18
R_{wp}	5.3%	6.3%
R_{Bragg}	6.2%	4.5%

[a]Anisotropic thermal factor used for the refinement.

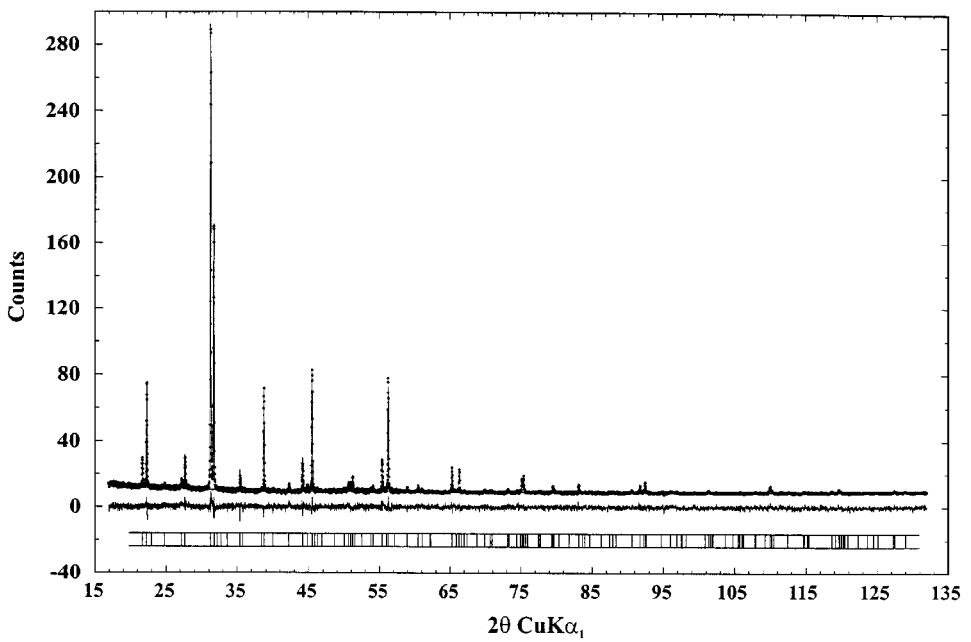

FIG. 8. $Bi_2Ba_2Fe_4O_{11}$ ($x = 0.5$): result of the Rietveld analysis of the XRPD diagram.

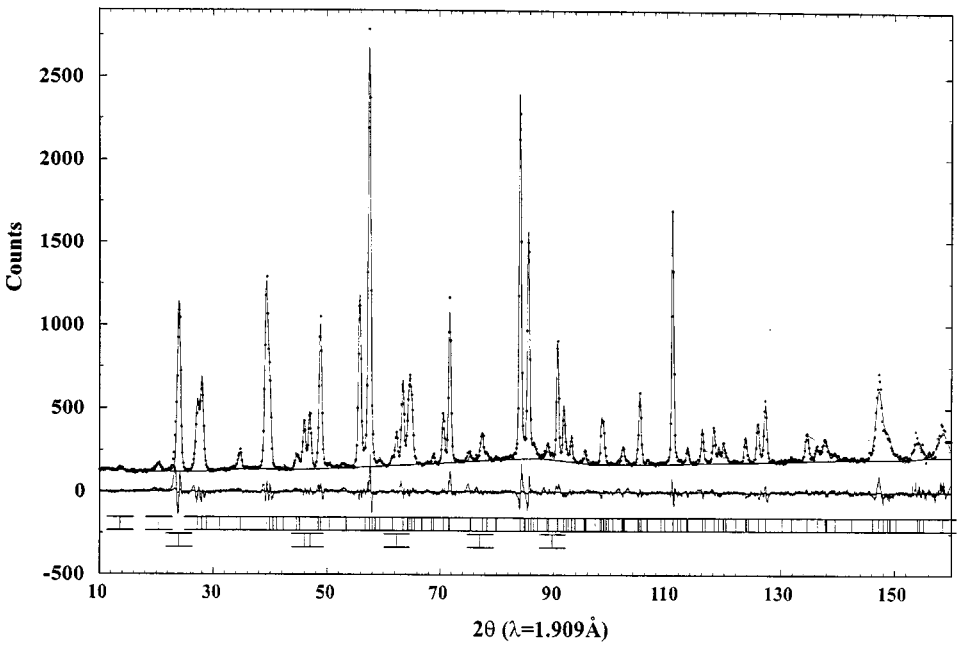

FIG. 9. $Bi_2Ba_2Fe_4O_{11}$ ($x = 0.5$): result of the Rietveld analysis of the NPD diagram (nuclear structure).

observed that a few images are observed in the model I and not in the model II, and inversely. Two examples of these univocal images are given, for the $x = 0.5$ sample, in Figs. 10a and 10b, where the white dots are correlated to the cation positions. In Fig. 10a (focus value close to -5 nm), the single row of the brighter dots corresponds to the $Fe(3)O_2$ rows (black arrow); in Fig. 10b (focus value close to -115 nm), this row of Fe(3) and the two surrounding rows of "Bi-rich" sites (groups of three arrows) appear as three adjacent rows of staggered dots, separated by two rows of "Ba-rich" sites. Such images allow one to select model II, with an iron atom at the origin. It can also be observed that if the layers sequence is perfect, in agreement with the $\mathbf{q} = 0.25$ value, local variations of the intensity suggest that the atom distribution is not really perfect; this is especially visible at the level of the Bi–Fe– Bi rows (Fig. 10b).

One [100] HREM image and the corresponding ED pattern, recorded for the $x = 0.45$ sample, are given in Fig. 11. One of the signatures of the modulation is clearly visible, through the irregular stacking of $3a_p$ and $4a_p$ spacing between two equivalent rows of atomic rows (some periodicities are denoted by black numbers in the left part of the image). It appears that the group of three rows of staggered dots, corresponding to the Bi–Fe(3)–Bi rows, are separated by two ($4a_p$) or one ($3a_p$) rows of white dots correlated to the "Ba-rich" sites. Here again, local variations of the contrast attest to the local atomic substitutions; the effect is more intense than the one observed in the quadruple perovskite and is sometimes extended to a complete atomic row.

TABLE 7
Interatomic Distances (Å) Calculated from Table 6

Ba(1)–O(1)	2.82(1)	(×4)	Bi(1)–O(1)	2.62(1)	(×4)
Ba(1)–O(4)	2.82(1)	(×4)	Bi(1)–O(4)	2.82(1)	
Ba(1)–O(2)	3.05	(×4)	Bi(1)–O(2)	3.28	(×4)
Ba(2)–O(2)	2.67(1)	(×4)	Bi(2)–O(2)	2.48(1)	(×4)
Ba(2)–O(5)	2.62(1)	(×1.5)	Bi(2)–O(5)	2.66(1)	(×1.5)
Ba(2)–O(5)	3.04(1)	(×1.5)	Bi(2)–O(5)	3.07(1)	(×1.5)
Ba(2)–O(3)	2.68(1)	(×1.5)	Bi(2)–O(3)	2.92(1)	(×1.5)
Ba(2)–O(3)	3.11(1)	(×1.5)	Bi(2)–O(3)	3.33(1)	(×1.5)
Fe(1)–O(1)	1.99(1)	(×4)	Fe(2)–O(2)	2.02(1)	(×4)
Fe(1)–O(4)	2.07(1)	(×2)	Fe(2)–O(4)	1.91(1)	(×1)
Fe(3)–O(3)	2.02(1)	(×3)	Fe(2)–O(5)	2.33(2)	(×0.75)
Fe(3)–O(5)	1.92(1)	(×1.5)			

THE MAGNETIC STRUCTURE

The analysis of the magnetic structure from NPD data was performed on the samples $x = 0.43$, $x = 0.45$, $x = 0.48$, and $x = 0.5$. For the incommensurate tetragonal members ($x = 0.45$ and $x = 0.48$) the refinements were made only considering the average perovskite cell and using antisotropic factors for the thermal parameters. For the member $x = 0.43$, the analysis was performed using the cubic space group *Pm3m*. In fact, a slight broadening in the base of the peaks at high angles suggests the existence of the tetragonal distortion observed in ED (5).

The results are presented only for the two members $x = 0.43$ and $x = 0.50$ (Fig. 12, Table 8 and Fig. 13, Table 9,

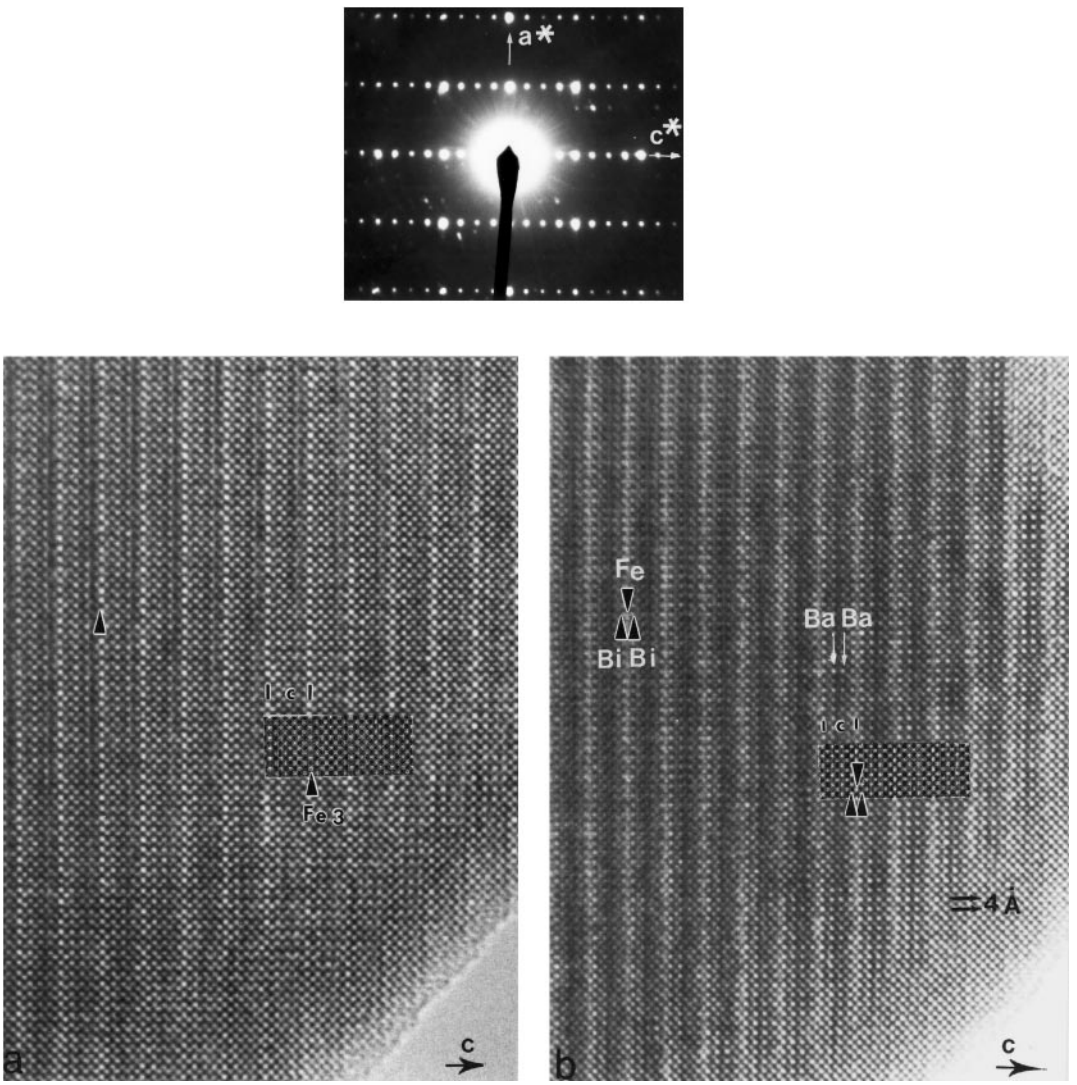

FIG. 10. (Top) $Bi_2Ba_2Fe_4O_{11}$: [100] ED pattern and two univocal [100] HREM images. The bright dots are correlated to the cation positions: (a) (Focus value close to -5 nm) the single row of the brighter dots corresponds to the Fe(3)–O_2 rows (black arrow). (b) (Focus value close to -115 nm) this row of Fe(3) and the two surrounding rows of "Bi-rich" sites (groups of three arrows) appear as three adjacent rows of staggered dots.

respectively) which correspond to the two limit members for which the magnetic coupling is established at room temperature. The study indicates that the magnetic ordering is the same for all the samples, and the extra magnetic reflections can be indexed using the propagation vector $\mathbf{k} = (\frac{1}{2}, \frac{1}{2}, \frac{1}{2})$ expressed in the perovskite cell; i.e., the propagation vector is reduced to $k = (\frac{1}{2}, \frac{1}{2}, 0)$ for the four-fold perovskite ($x = 0.5$).

The magnetic structure can be described as a stacking sequence $+, -$ along the **c** direction of antiferromagnetic (AF) planes corresponding to a $2a_p$ periodicity. Within the AF planes, the iron spins, lying perpendicular to the **c** axis, are antiferromagnetically coupled along the [110] direction. The canting of the magnetic moment, observed by magnetic measurement (5), is too weak to be refined with the neutron data. For the members $x = 0.43$ to $x = 0.48$, this ordering leads to a quadrupling of the magnetic cell, compared to the nuclear one, with $a_{magn} = a_{nucl}\sqrt{2}$ and $c_{magn} = 2c_{nucl}$. For the member $x = 0.5$, having a nuclear cell in $a_p \times a_p \times 4a'_p$, the magnetic cell has only a double volume in $a_p \times \sqrt{2} \times a_p\sqrt{2} \times 4a_p$. A schematic representation of the iron spins are displayed in Fig. 14 for the member $x = 0.5$.

CONCLUDING REMARKS

The Rietveld analyses of both XRPD and NPD data have allowed us to evidence the structural relationship existing inside the solid solution $[Ba_{2-3x}Bi_{3x-1}][Fe_{2x}Bi_{1-2x}]$

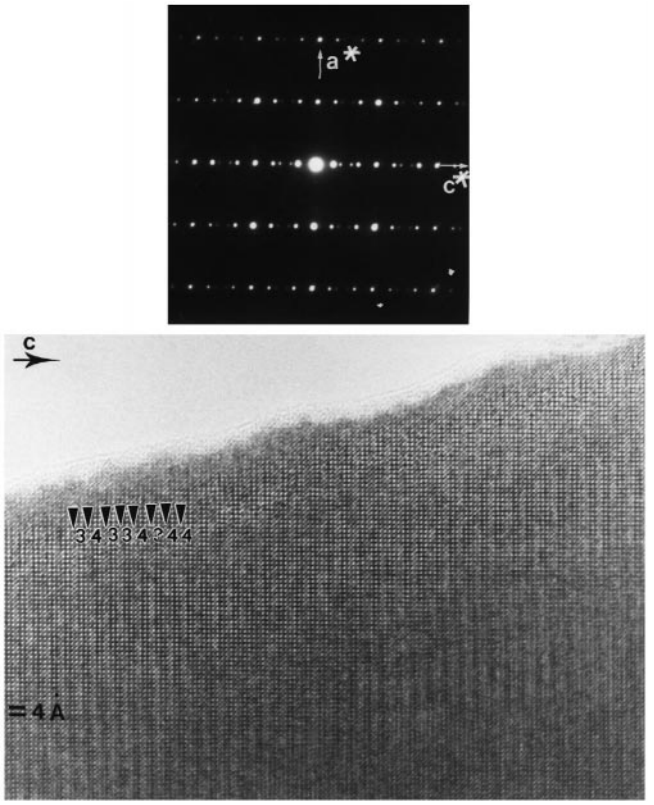

FIG. 11. [1 0 0] HREM image and ED pattern for the $x = 0.45$ sample with an irregular stacking of $3a_p$ and $4a_p$ spacings.

TABLE 8
$x = 0.43$ Member: Structural Parameters Obtained from Neutrons D Data (Magnetic and Nuclear Structure)

SG: *Pm*3*m* (No. 221), $a = 4.0506(1)$ Å

Atom	x	y	z	Occup.	B (Å^2)
Ba(1)	0.5	0.5	0.5	0.7	4.4(2)
Bi(1)	0.5	0.5	0.5	0.3	4.4(2)
Fe(1)	0	0	0	0.9	2.1(1)
Bi(2)	0	0	0	0.1	2.1(1)
O(1)	0	0	0.5	0.89	2.2(1)

Note. Propagation vector: (1/2, 1/2, 1/2). Magnetic moment: $|M_{(x,y,z)}| = 4.1(1)$. $\chi^2 = 3.8$, $R_{wp} = 17.9\%$, $R_{Bragg} = 6.7\%$, $R_F = 4\%$, $R_F - \text{Magn} = 10.5\%$.

$O_{2+3x/2}$ ($040 \leq x \leq 0.5$) for both nuclear and magnetic structure. Though the structural analysis is still incomplete, the use of the superspace formalism gives a good idea of the cationic ordering between Ba and Bi. From this study, it results that a true Ba/Bi statistical occupancy of a single *A* site does not appear in the present compounds. There exists a particular ordering between Ba and Bi which can be described in a four-dimensional periodic crystal.

Some static disorder phenomena, mostly attached to the Bi atoms, have also been evidenced. Such disorder

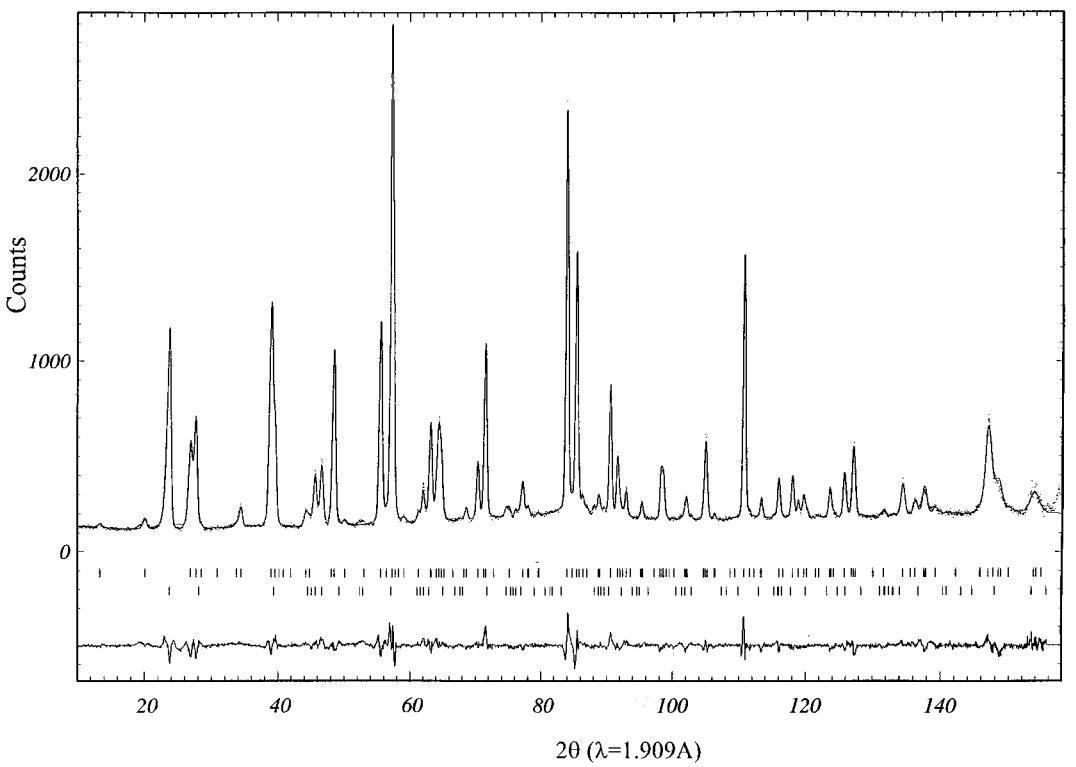

FIG. 12. $Bi_2Ba_2Fe_4O_{11}$ ($x = 0.5$): result of the Rietveld analysis of the NPD diagram (the first row of bars corresponds to the nuclear reflections and the second one to the magnetic reflections).

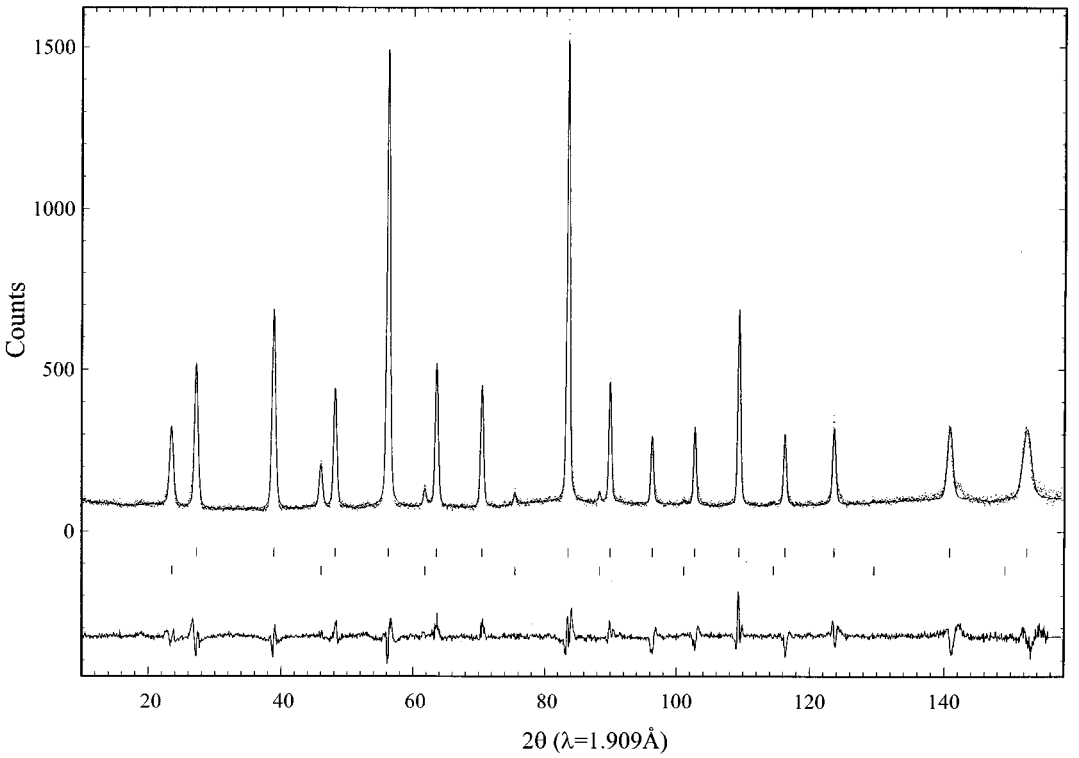

FIG. 13. $x = 0.43$: result of the Rietveld analysis of the NPD diagram (the firt row of bars corresponds to the nuclear reflections and the second one to the magnetic reflections).

phenomena are commonly observed for Bi atoms in the family of the so-called Bi–2212 oxides as well as in Aurivillius phases of the type $Bi_2ANb_2O_9$ where A = Ba, Sr, Ca (14). For the latter compounds, similar mixed Ba/Bi sites are observed with high thermal factors, but ordering between Ba and Bi atoms have not been observed.

TABLE 9
$x = 0.5$ Member: Structural Parameters Obtained from Neutrons D Data (Magnetic and Nuclear Structure)

SG: $P4/mmm$ (No. 123), $a = 3.9802(2)$ Å, and $c = 16.376(1)$ Å

Atom	x	y	z	Site	Occup.	B(Å^2)
Ba(1)	0.5	0.5	0.116(1)	2*h*	0.75	3.3[a]
Bi(1)	0.5	0.5	0.116(1)	2*h*	0.25	3.3[a]
Bi(2)	0.5	0.5	0.356(1)	2*h*	0.75	4.9[a]
Ba(2)	0.5	0.5	0.356(1)	2*h*	0.25	4.9[a]
Fe(1)	0	0	0	1*a*	1	1.0[a]
Fe(2)	0	0	0.2441(6)	2*g*	1	1.3[a]
Fe(3)	0	0	0.5	1*b*	1	3.7[a]
O(1)	0.5	0	0	2*f*	1	1.5[a]
O(2)	0.5	0	0.2621(6)	4*i*	1	2.2[a]
O(3)	0.5	−0.086(5)	0.5	4*o*	3/8	2.5(6)
O(4)	0	0	0.127(1)	2*g*	1	1.8[a]
O(5)	0.081(8)	0	0.384(1)	8*s*	3/16	1.6(8)

Note. Propagation vector: (1/2, 1/2, 0). Magnetic moment: $|M_{(x,y)}| = 3.4(2)$, $|M_z| = 0$. $\chi^2 = 3.42$, $R_{wp} = 10.7\%$, $R_{Bragg} = 4.4\%$, $R_F = 3.8\%$, $R_F - \text{Magn} = 6.4\%$.

[a]Anisotropic thermal factor used for the refinement.

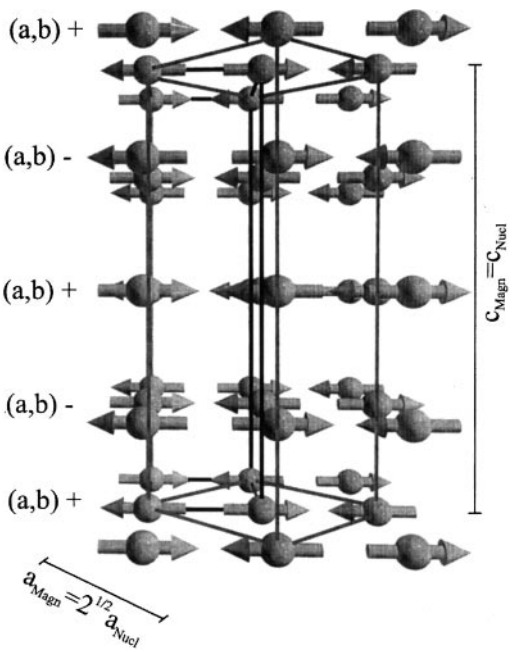

FIG. 14. Schematic representation of the iron spins for $x = 0.50$.

ACKNOWLEDGMENTS

The authors would like to thank the CPS Laboratory at the Ecole Centrale of Paris for giving us the possibility to use their prototype diffractometer and, especially, D. G. Baldinozzi for the data collection.

REFERENCES

1. J. B. Goodenough, "Magnetism and the Chemical Bond." John Wiley & Sons, New York, London, 1963.
2. C. N. R. Rao and B. Raveau, "Transition Metal Oxides," 2nd ed. Wiley–VCH, New York, 1998.
3. J. B. Goodenough and J. M. Longo, *in* "Magnetic order and Other Properties of Oxides and Related Compounds" (K. H. Hellwege and O. Madelung, Eds.), Landolt-Börnstein, New Series, Group III, Vol. 4a. Springer Verlag, Berlin, 1970.
4. M. Zanne, C. Gleitzer, and J. Aubry, *J. Solid State Chem.* **14,** 160 (1975).
5. Ph. Boullay, M. Hervieu, N. Nguyen, and B. Raveau, *J. Solid State Chem.* **147,** 45 (1999).
6. M. T. Anderson, K. R. Poeppelmeir, J-P. Zhang, H-J. Fan, and L. D.Marks, *Chem. Mater.* **4,** 1305 (1992).
7. A. Gormezano and M. T. Weller, *J. Mater. Chem.* **7,** 771 (1993).
8. K. B. Greenwood, G. M. Sarjeant, K. R. Poeppelmeir, P. A. Salvador, T. O. Masson, B. Dabrowski, K. Rogacki, and Z. Chen, *Chem. Mater.* **7,** 1355 (1995).
9. J. F. Berar, Presented at Satellite meeting on powder diffraction, XVth Congress of International Union of Crystallography, July 1990.
10. J. Rodriguez-Carjaval, Presented at Satellite meeting on powder diffraction, XVth Congress of International Union of Crystallography, July 1990.
11. T. Jansen, A. Janner, A. Looijenga, and P. M. de Wolff, "International Tables for Crystallography" (A. J. C. Wilson, ed.), Vol. C797. Kluwer Academic Publishers, Dordrecht, 1992.
12. N. Jakubowicz, O. Pérez, D. Grebille, and H. Leligny, *J. Solid State Chem.* **139,** 194 (1998).
13. B. Dam and A. Janner, *Acta Crystallogr. B* **42,** 69 (1986).
14. S. M. Blake, M. J. Falconer, M. McCreedy, and Ph. Lightfoot, *Mater. Chem.* **7,** 16098 (1997).